PATENT ABSTRACTS OF JAPAN

(11)Publication number : 61-020377

(43)Date of publication of application : 29.01.1986

(51)Int.Cl.   H01L 39/22

(21)Application number : 59-140512   (71)Applicant : HITACHI LTD

(22)Date of filing :   09.07.1984   (72)Inventor : NISHINO JUICHI

(54) SUPERCONDUCTIVE CIRCUIT

(57)Abstract:

PURPOSE: To obtain the titled device which has a high integration degree and stable action and can be manufactured with high yield, by a method wherein a thin film of crystal with a (1,0,0) plane or polycrystal oriented mainly to a (1,0,0) plane is selectively formed and used for a superconductive electrode, in the crystal of a superconductor having a crystal structure of NaCl structure.
CONSTITUTION: An NbN thin film is formed on an MgO single crystal substrate 1 of (1,0,0) plane by reactive sputtering. The NbN thin film is made of polycrystal of (1,0,0) plane strongly oriented to the (1,0,0) plane or to this direction by following the crystallinity of the MgO substrate. This NbN thin film is processed into the superconductive electrode 2 by Ar ion etching with a mask of a photo resist pattern. Next, an interlayer insulation film 3 made of an SiO2 thin film and having an aperture is formed. The surface of the superconductive electrode 2 exposed in this aperture is oxidized with Ar plasma into a tunnel barrier layer 4; successively, a superconductive electrode 5 made of Pb-5wt% In alloy is formed.
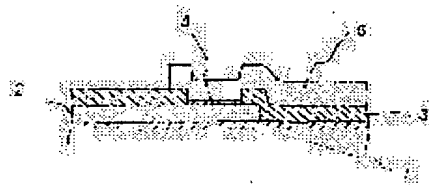
LEGAL STATUS

[Date of request for examination]

[Date of sending the examiner's decision of rejection]

[Kind of final disposal of application other than the examiner's decision of rejection or application converted registration]

[Date of final disposal for application]

[Patent number]

[Date of registration]

[Number of appeal against examiner's decision of rejection]

[Date of requesting appeal against examiner's decision of rejection]

[Date of extinction of right]

　　　　　明　　細　　書
　発明の名称　超電導回路
　特許請求の範囲
1．極低温において動作し、配線又は電極の一部
　又は全部の材料は結晶構造がNaCℓ（岩塩）構
　造の超電導薄膜を用いて成り、かつ該超電導薄
　膜は（1，0，0）面の結晶あるいは主として
　（1，0，0）面に配向した多結晶体を用いて
　成ることを特徴とする超電導回路。
2．特許請求の範囲第1項記載の超電導回路にお
　いて、前記NaCℓ（岩塩）構造の超電導薄膜は
　NbN，MoNより選ばれた少なくとも1材料
　であることを特徴とする超電導回路。
3．特許請求の範囲第1項もしくは第2項記載の
　超電導回路において、前記超電導薄膜を形成す
　る下地材料はMgO，NaCℓ，S1より選ば
　れた1材料から成り且つ前記超電導薄膜の形成
　面が（1，0，0）面の単結晶あるいは（1，
　0，0）面に配向した多結晶体を用いて成るこ
　とを特徴とする超電導回路。

　発明の詳細な説明
　〔発明の利用分野〕
　本発明は、超電導状態の得られる極低温で動作
する超電導回路に係り、高集積度でかつ動作が安
定な超電導回路を高い製造歩留りで作製すること
ができる構造の超電導回路に関する。
　〔発明の背景〕
　極低温で動作する超電導回路、特にジョセフソ
ン接合を用いた回路において、その超電導電極あ
るいは配線の材料に結晶構造がNaCℓ構造の超
電導薄膜を用いることは、例えばIEEE Trans.
Magnetics Mag-15，314（1981年）におけ
るKosaka等による"Fabrication of NbN／Pb
Josephson Tunnel Junctions with a novel
integration method"と題する文献に論じられて
いる通り公知の技術である。例えばNbN は超電導
転移温度が14～15Kと他の超電導体に比べて
高いため温度ゆらぎに対して回路動作が安定であ
るという利点がある。NbN薄膜はJournal of
Applied Physics 54，6509（1983年）における

Bacon等の"Properties of NbN thin films deposited on ambient temperature substrates." と称する文献に記載されたる様に主として反応性スパッタリング法によって作製されることが知られている。しかし従来は結晶性の良い薄膜が得られなかったため、NaCl構造の超電導薄膜の結晶性、配向性と、薄膜の表面状態との関係、特に表面自然酸化膜厚との関係については全く知見が得られていなかった。

一方、NbN等を用いた超電導回路は上記特長があるものの、特性のバラツキが多く、再現性に問題があり、製造歩留りも高くなかった。

〔発明の目的〕

本発明は、高集積度で動作が安定であり且つ高い歩留りで製造することができる超電導回路を提供することにある。

〔発明の概要〕

本発明では、結晶構造がNaCl構造の超電導体の結晶において薄膜として得易い表面が（1，0，0）面と（1，1，1）面と平行な薄膜のう

ち、特に酸化速度の遅い（1，0，0）面の結晶あるいは主として（1，0，0）面に配向した多結晶薄膜を選択的に形成し超電導電極に用いることによって、超電導相互の接続を容易に形成でき、またジョセフソン接合のトンネル障壁層を制御性良く形成できるように構成したものである。

本発明者らはNbN等を用いた超電導回路のバラツキについて検討した結果、超電導薄膜の表面自然酸化膜は、超電導体相互の超電導接続やジョセフソン接合のトンネル障壁層を形成する際にその製造の制御性に大きく影響するため、その性質を良く制御する必要があることが新たに分つたのである。本発明はこの発見に基づいて、さらに研究を進めた結果得られたものである。

〔発明の実施例〕

以下、実施例を参照して本発明を詳細に説明する。（1，0，0）面のMgO単結晶基板1上に反応性スパッタリング法により厚さ約200nmのNbN薄膜を形成した。このときの基板温度は400℃とし、スパッタリングには圧力2Paの

Ar＋30％N₂ガスを使用した。このNbN薄膜はMgO基板の結晶性を引き継いで（1，0，0）面あるいはこの方向に強く配向した多結晶より成る。このNbN薄膜をホトレジストのパターンをマスクとしてArイオンエッチング法により加工し、超電導電極2とした。次いで厚さ300nmのSiO薄膜より成り、開口部を有する層間絶縁膜3を形成した。この開口部内に露出した超電導電極2の表面を圧力1paのAr＋5％O₂ガスを用いたプラズマによって酸化し厚さ3～4nmのトンネル障壁層4を形成し、引き続いて厚さ約50nmのPb－5vt％In合金より成る超電導電極5を形成した。このようにして形成されたジョセフソン接合の一部を第1図に示す。このジョセフソン接合は、下側の超電導電極1の結晶方位がそろっているためにトンネル障壁層4であるNb酸化物膜が均一であり、しかも（1，0，0）面のNbN結晶は酸化速度が遅くトンネル障壁層4を形成する前にプロセスの途中で生じる自然酸化物は高々1nmであって均一であるために、製

作の制御性を高くすることができた。

第2図に、本発明の第2の実施例を示す。第1の実施例と同様の基板1上に超電導電極2を形成する。次いで超電導電極2の表面をArイオンを用いて約10nmエッチングした後に、NbNより成る超電導電極6を形成した。このようにして2つの超電導電極の接続を形成したところ、超電導電極2は主に（1，0，0）面のNbN結晶より成るために、接続を形成する前に生じる自然酸化膜が高々1nmと薄く、従ってArイオンによる表面清浄化処理を極めて再現性良く行うことができた。またその結果として、超電導接続を流れる超電導臨界電流の再現性を高めることができた。

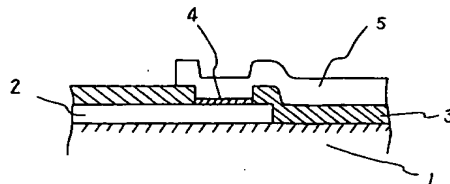これらの実施例では基板に（1，0，0）面のMgO結晶を用いたが、（1，0，0）面のSi，NaClを用いても同様の結果を得ることができた。

また、上記実施例では、超電導体としてNbNを用いたがMoNを用いても同様の結果が得られ

た．

ル障壁層．

代理人　弁理士　高橋明

〔発明の効果〕

　以上述べたように、本発明によれば、極低温で動作する超電導回路において、これを構成する超電導電極の表面に製造途中で生じる自然酸化膜厚を高々1.0 nmにおさえることができ、しかもその厚さは結晶面がそろっているために均一であるので、膜表面の清浄化処理を従来の半分程度にすることができ、しかもその再現性を高くすることができるほかに、ジヨセフソン接合のトンネル障壁層を形成する場合には、超電導電極表面の結晶方位がそろっているために、酸化物トンネル障壁層の均一性が良くなり、従ってジヨセフソン接合の特性の均一性と再現性を向上させることができた。

図面の簡単な説明

　第1図は本発明の一実施例における超電導回路の一部を示す断面図、第2図は本発明の他の実施例における超電導回路の一部を示す断面図である。

1…基板、2，5，6…超電導電極、4…トンネ
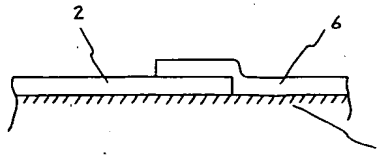
第 1 図

第 2 図

Microstructure and Superconductivity in Epitaxial MgO/NbN Multilayers

Shiro NAGAOKA, Katsuyoshi HAMASAKI[†], Tsutomu YAMASHITA[†]
and Toranosuke KOMATA[††]

TOSOH Corporation, Advanced Materials Research Laboratory, Hayakawa, Ayase 252
[†]Department of Electronics, Nagaoka University of Technology, Kamitomioka, Nagaoka 940-21
[††]Department of Electronics, Kanazawa Institute of Technology, Nonoichi, Ishikawa 921

大体 ×のくらい.

The aim of this investigation is to achieve high transition temperature, low resistivity films under conditions suitable for use in all-NbN Josephson junction fabrication. For this purpose, the heteroepitaxy of NbN on MgO films is investigated. For substrate temperature of 200°C or thereabouts, polycrystalline MgO films of (200) orientation were formed on (100) silicon, (1$\bar{1}$02) α-Al$_2$O$_3$, and fused silica. Based on XTEM, HEED and X-ray data, heteroepitaxial growth (($(100)_{NbN} // (100)_{MgO}$) was obtained in NbN films and NbN/MgO/NbN trilayers deposited on (200) oriented MgO films. The epitaxial NbN films of 10 nm thickness had high transition temperatures of about 14 K, and relatively low residual resistivities of less than 200 $\mu\Omega \cdot$cm. Using the GL relationships, we calculated the Ginzburg-Landau parameters, $\lambda(0)$ and ξ, of our NbN films in the dirty limit. The calculated $\xi(4.2$ K$)$ and $\lambda(0)$ are ~ 4.5 nm and ~ 300 nm, respectively.

KEYWORDS: Josephson device, MgO/NbN multilayer, epitaxy, coherence length, penetration depth

§1. Introduction

Because of the potential of niobium nitride (NbN) for Josephson junctions, it has attracted a great deal of attention. So far, many studies have been reported on NbN junctions where most of the NbN films were reactively sputtered in ambients of Ar + N$_2$ mixture.

Many problems fundamental to the preparation of high quality tunnel junctions are strongly related to interface morphology in the superconducting electrodes and the insulator layer (barrier). One of the problems is that the superconducting coherence length, ξ, of NbN is at least a factor of 2 lower than that for Nb. For NbN and Nb, $\xi(4.2$ K$)$ is (4-7) nm and (10-30) nm,[1] respectively. Hence, reliable process technology is necessary in order to prepare the high T_c NbN layers which are first deposited, i.e., layers adjacent to the insulator layer with thickness characterized by ξ.

One of the principle procedures permitting formation of ultrathin NbN layers with characteristics similar to those of bulk materials is heteroepitaxial growth. NbN and MgO have a B1 (sodium chloride) structure. The lattice constant of NbN is 0.438 nm. The lattice constant of MgO, 0.421 nm, is only 4% smaller than NbN. Hence, it is possible to study the preparation conditions for heteroepitaxial growth of NbN deposited on MgO crystals.

Much research has been carried out on the formation of heteroepitaxial layers of NbN. In these reports, for formation of epitaxial NbN layers, the authors used cleaved MgO as the substrate.[2-6] However, not much attention has been paid to Josephson device fabrication because of the roughness of the cleaved MgO surface. Recently, we developed a novel process for preparing heteroepitaxial layers of NbN which is suitable for fabrication of various Josephson devices.[7,8] The most important point in this technology is the preparation of highly oriented MgO films by rf magnetron sputtering. As mentioned in earlier reports,[7] we have successfully prepared epitaxial NbN deposited on (200) oriented MgO layers. Talvacchio et al.[9,10] also recently reported epitaxial growth of NbN/MgO, or Mg$_{1-x}$Ca$_x$O/NbN layered structures. They obtained high-quality junctions with high gap voltages.

In this paper, we describe the sequence of multilayer deposition and the results of structural analysis of MgO/NbN bilayers and MgO/NbN/MgO/NbN tetralayers, based on cross-sectional transmission electron micrograph (XTEM), high energy electron diffraction (HEED), and X-ray diffraction (XRD) data. The superconducting properties of epitaxial NbN films are also investigated.

§2. Film Preparation

One problem in choosing a suitable substrate is that impurities may diffuse from the substrate and contaminate the films. MgO exhibits extremely high thermodynamic stability below 300°C, that is to say, its decomposition pressure is relatively low. Hence, MgO deposited by sputtering with an MgO target will be in congruent evaporation, and may be stoichiometric. Our hope is that the orientation of MgO is independent of deposition conditions (background pressure, substrate temperature, rf power density and the like), as reported in NaCl films.[11]

MgO films were deposited by rf magnetron sputtering in a multitarget sputtering system (ANELVA 430 H) with a cryo- or diffusion-pump. The sputtering gases were high-purity (99.9995%) Ar, N$_2$, and an Ar + N$_2$ mixture. To investigate the effect of the crystallinity of substrate materials on the crystallite orientation of MgO films, series of runs were conducted using different substrates. The substrates used were (100) silicon, (1$\bar{1}$02) α-Al$_2$O$_3$, and fused silica. The substrate temperature was in the range of (150-210)°C. The background pressure before deposition was typically 2×10^{-4} Pa. The target was a disk of hot-pressed MgO of 99.99% purity. Most films were deposited at a rate of ~ 9.5 nm/min, where the thickness of films thicker than 40 nm was measured by a

surface profilometer (Tencor, Inc. Model α-step 200).

Following the MgO deposition, a thin NbN layer was sequentially deposited onto the predeposited MgO layer on the substrates without breaking the vacuum. NbN films were produced by reactive rf magnetron sputtering in 2.4 Pa of Ar+($\sim$9%)N_2 mixture. The substrate temperature was about 210°C, and the sputtering rate for an rf power density of 5.1 W/cm^2 was $\sim$80 nm/min in Ar+($\sim$9%)N_2 mixture. The film resistance as a function of temperature was measured using a four-probe arrangement. A calibrated silicon diode (Lake Shore Cryotronics, Inc.) was used as a temperature sensor, with a measurement accuracy of ±0.1 K in the 4–20 K range.
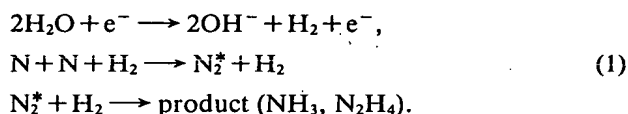
§3. Structural Analyses

3.1 X-ray diffraction

Figure 1 presents the XRD results for 80 nm thick MgO films deposited onto various substrates using the ANELVA 430 H system with a diffusion pump. The films were deposited in rf sputtering gas of pure Ar, and at a total pressure of $\sim$4.2 Pa. Patterns (a)–(c) in Fig. 1 are characteristics of films deposited on (100) silicon, ($1\bar{1}02$) α-Al_2O_3, and fused silica, respectively. All traces in Fig. 1 clearly indicate that $(200)_{MgO}$ is the preferred crystallite orientation. As can be seen from Fig. 1, the full width at half maximum (FWHM) for the MgO film deposited on the (100) silicon is somewhat narrower than that on fused silica.

In a recent study in our laboratory, an anomalous dependence of the intensity of line $(200)_{MgO}$ on sputtering ambients was observed.[12] Figure 2 shows the XRD data for MgO films deposited onto (100) silicon using the

cryo-pump system (ANELVA 430 H). The partial pressure P_{N2} of N_2 in Ar gas was changed over a range from 0% to 100%. The films were deposited at a total pressure of $\sim$1.5 Pa, and rf power density of 2.6 W/cm^2. In all films, the sputtering time is 10 min, but does not give the same thicknesses. A clear trend of increasing intensity of line (200) is observed as P_{N2} is increased. This trend was also observed for MgO films deposited using the diffusion-pump system (ANELVA 430 H).

On this subject, the following mechanism can be proposed. As mentioned by Sugiyama et al.,[13] MgO revealed catalytic activity in the plasma synthesis of ammonia from H_2–N_2 mixed gas. Also, in N_2 plasma in which water vapor is mixed, the following reactions take place.[14]

$$2H_2O + e^- \longrightarrow 2OH^- + H_2 + e^-,$$

$$N + N + H_2 \longrightarrow N_2^* + H_2 \qquad (1)$$

$$N_2^* + H_2 \longrightarrow \text{product (NH}_3, N_2H_4).$$

As pointed out by Sugiyama et al.,[13] the reaction occurs on the surface of MgO. Excited nitrogen molecules are absorbed on MgO, and the MgO surface becomes a nitride which is; at the same time, reduced by hydrogen atoms. In their results, the ESCA spectrum showed the presence of magnesium nitride but the amount of the nitride was negligible. Although the mechanism whereby the nitrogen ion responds to increase in the intensity of line (200), as shown in Fig. 2, is not fully understood, our results might be explained by the generation of very small amounts of magnesium nitride, or magnesium hydroxide.

MgO and Al_2O_3 are attractive tunnel-barrier materials due to their good thermodynamic stability. From this point of view, NbN/MgO/NbN trilayers have been sequentially deposited on MgO films. The normalized peak intensity of $(200)_{NbN}/((111)_{NbN}+(200)_{NbN})$ is a relative index of the crystallite preferred orientation of heteroepitaxial NbN. Figure 3 is a plot of this value as a function of the thickness of thin MgO overlayers on NbN base electrodes. These thin overlayers act as a tunnel barrier. The preferential orientation of (200) planes in MgO (underlayer)/NbN/MgO(barrier)/NbN tetralayers is independent of the thickness of thin MgO barriers.
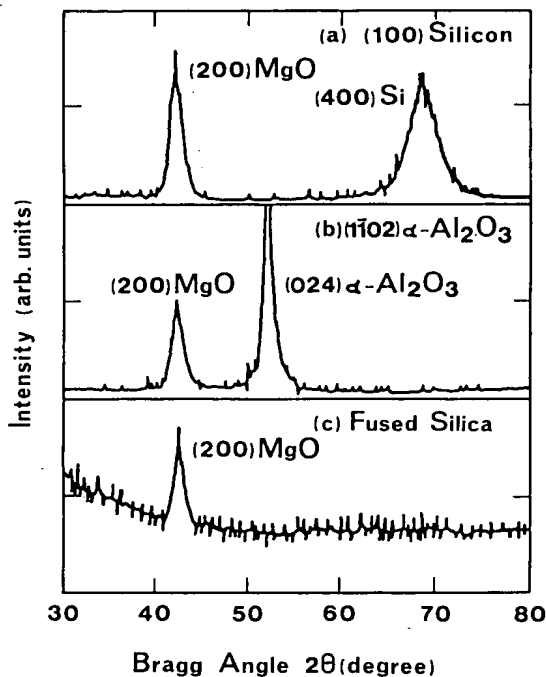
Fig. 1. Portion of X-ray diffractometer traces of MgO films deposited on three kinds of substrates. Deposition conditions are as follows: (1) substrate temperature: $\sim$210°C, (2) rf power density: $\sim$2.6 W/cm^2, (3) a total pressure: $\sim$4.2 Pa, (4) the sputtering rate: $\sim$4 nm/min.
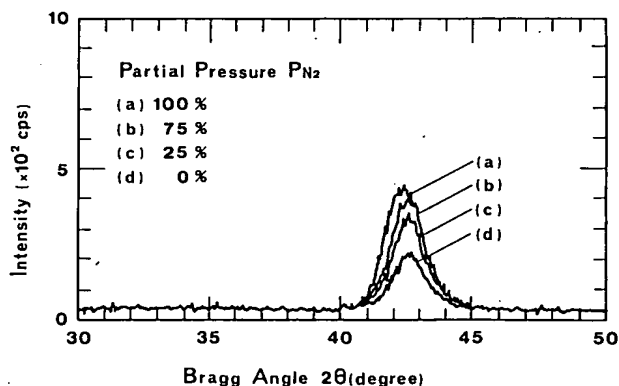
Fig. 2. X-ray diffractometer traces of MgO thin films.
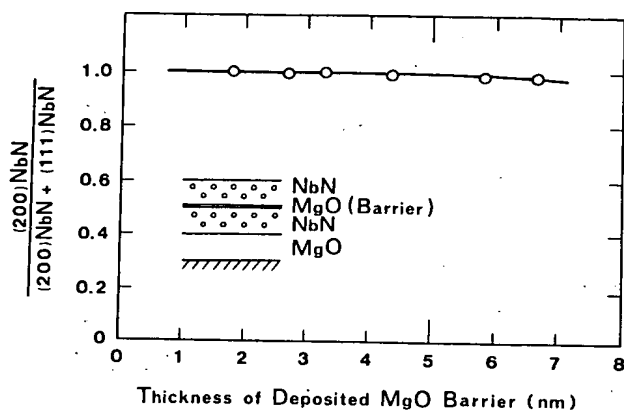
Fig. 3. Normalized peak intensity of $(200)_{NbN}$ line versus the thickness of MgO barrier layers. The MgO underlayers were deposited at ~150°C, and NbN/MgO/NbN trilayers were deposited at ~210°C.

3.2 TEM and HEED in cross section

In order to obtain more information about film growth, microstructure characterization was done by SEM, XTEM and HEED.[15] In the case of TEM, a relatively new sample preparation technique was used whereby cross sections could be observed, providing detailed insight into the heteroepitaxial growth structure. A sample for XTEM observations was prepared first by sectioning the Si wafer perpendicular to the MgO/NbN multilayer, as shown in Fig. 4. Then, the wafer was mechanically polished and locally etched by an Ar-ion beam. The ultimate thickness at the Ar-ion etched portion was in the range from 10 to 100 nm. The XTEM observation was done by means of a Nihondenshi electron microscope (JEM-200FX).

Figure 5(a) is a SEM photograph of a heteroepitaxial NbN/MgO/NbN on MgO film in cross section, and (b) is a lattice image of a (200) plane of the MgO base layer.
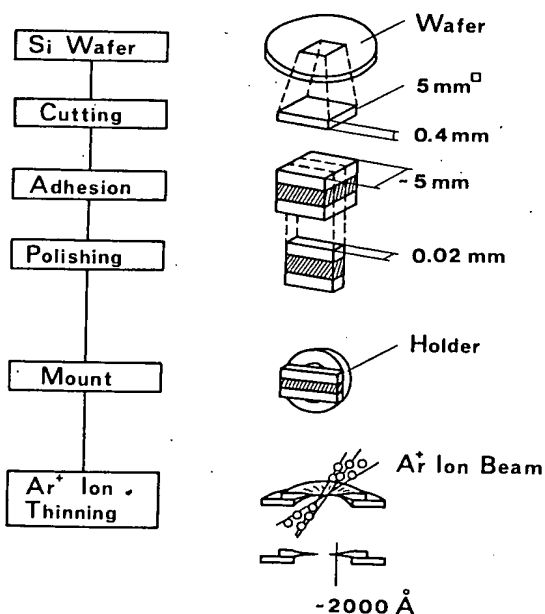
For the base MgO layer, a columnar structure has grown perpendicularly to the Si substrate. The grain diameter was in the range of 5 nm to 10 nm. The diffraction stripes of the MgO(200) plane in Fig. 5(b) are almost parallel to the Si substrate surface, but inclination of the (200) plane is evident at some points. The MgO//NbN interface is not smooth but has a roughness of about 10 nm between grain tops and grain boundary edges.

Figure 6 shows a HEED pattern from the

(a)

(b)

Fig. 4. Preparation of a sample for XTEM and HEED.
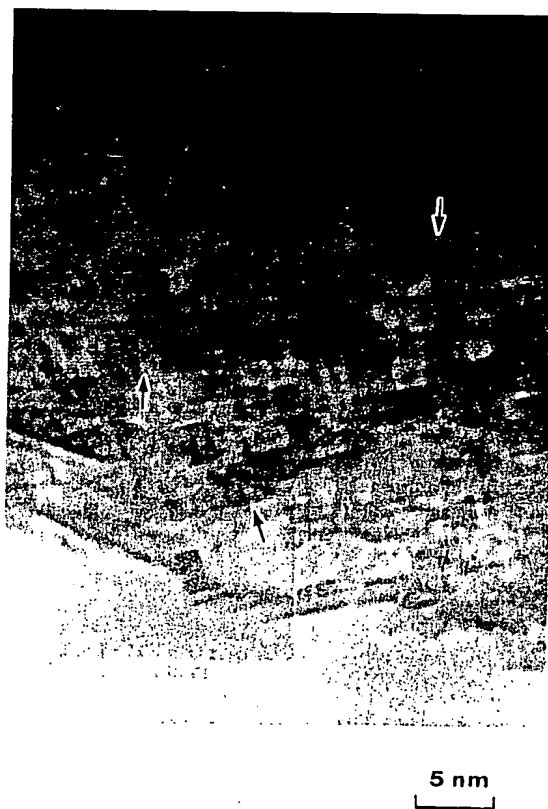
Fig. 5. (a) SEM photograph of heteroepitaxial NbN/MgO/NbN on MgO underlayer, and (b) lattice image of the (200) plane of the MgO underlayer.

MgO/NbN/MgO/NbN tetralayer in cross section, as shown in Fig. 5(a). The accelerating potential was 200 kV and the distance from the sample to the camera was 120 cm. The $(200)_{MgO}$ and $(200)_{NbN}$ diffraction spots with no streaks are observed. Both the (200) plane of MgO and that of NbN films are nearly parallel to the substrate surface. The sharpness of these spots and their orientation show conclusively that the NbN grows epitaxially on the MgO underlayer. However, Fig. 6 also shows discon-
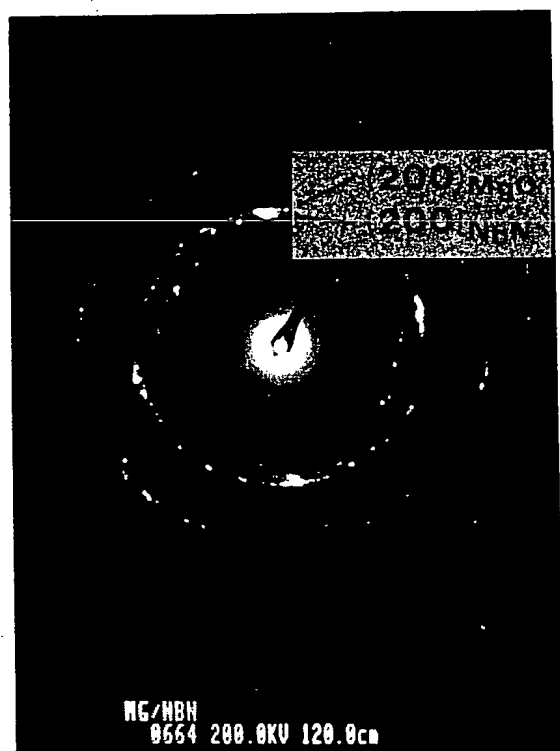
tinuous rings due to somewhat randomly oriented grains.

The dark-field micrographs of the same region of the sample as shown in Fig. 6 are given in Figs. 7(a), 7(b) and 7(c). The bright portions in these figures satisfy the diffraction conditions of (200) planes of cubic NbN and MgO. Changing the tilt angle of the sample to incident electron beam over a range from 0° to 10°[15] and observing the bright portions in the dark-field micrographs, we confirm the polycrystalline epitaxy in the whole cross section of the MgO/NbN/MgO/NbN tetralayer. Thus the polycrystalline epitaxial growth of NbN on MgO thin film is evident, as was the case for the NbN film (single-crystal epitaxy) formed on cleaved MgO; but it is not clear whether the uniformity of coverage of MgO barrier layers on base NbN could be good.

§4. Electrical Properties

NbN films formed on MgO films were characterized by their transition temperature T_c, and residual resistivity $\rho_0(20\ K)$. Figure 8 illustrates the T_c and $\rho_0(20\ K)$ vs the film thickness of NbN. All films were prepared in $Ar + (\sim 9\%)N_2$ mixture, and the thickness of MgO underlayers was about 150 nm. Although many films were analyzed by Auger spectroscopy, in most films, oxygen and carbon were not detected in NbN.[16] Hence, impurity is not a major factor contributing to the electrical properties of our films. In Fig. 8 T_c's remain 15–16 K when the NbN films are thicker than 30 nm. The T_c of 10 nm thick NbN films is about 14 K or thereabouts, and $\rho_0(20\ K) < 200\ \mu\Omega \cdot cm$. The best resistivity in 10 nm thick NbN films was about 80 $\mu\Omega \cdot cm$. The T_c and $\rho_0(20\ K)$ for ultrathin films (thickness < 20 nm) are somewhat better than those reported by Gavaler[17] and Igarashi et al.[18] The Ginzburg-Landau (GL) penetration depth for the BCS weak coupling case in the dirty limit, $\lambda_{GL}^d(T)$, is determined by the normal state resistivity and the transition temperature.[19]
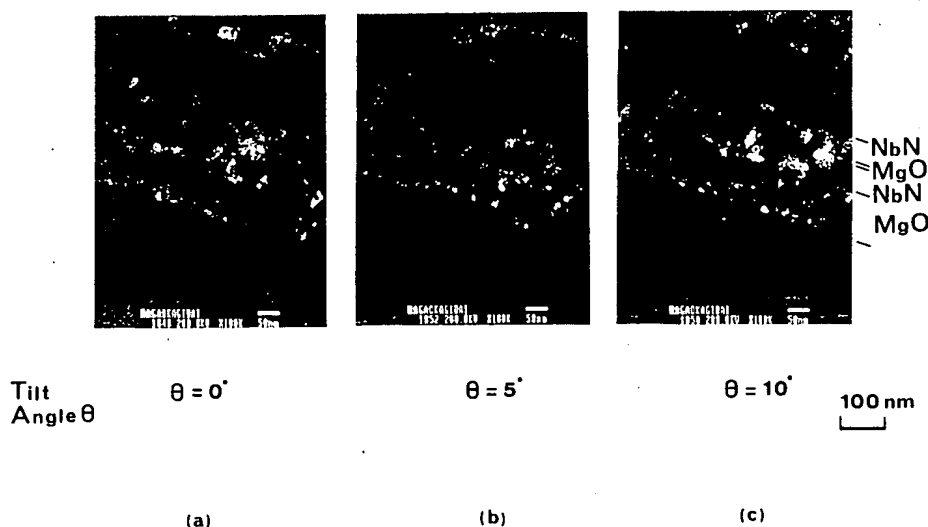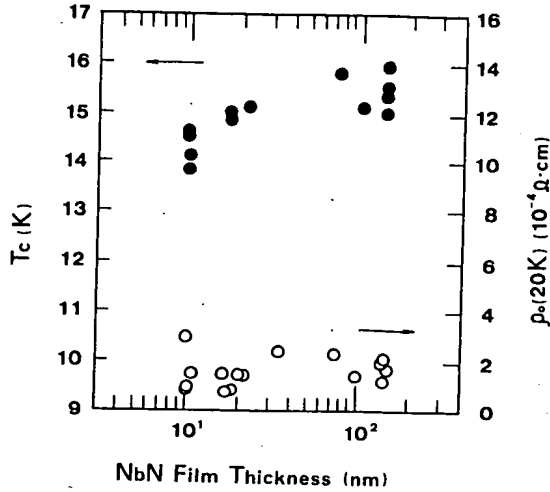

Fig. 6. HEED pattern from the MgO/NbN/MgO/NbN tetralayer. The $(200)_{MgO,NbN}$ diffraction spots with no streaks are observed.

Tilt Angle θ	θ = 0°	θ = 5°	θ = 10°	100 nm
	(a)	(b)	(c)	

NbN
MgO
NbN
MgO

Fig. 7. XTEM dark field images of a MgO/NbN/MgO/NbN tetralayer. The tilt angle, 2θ, to incident electron beam is: 0°, 5°, and 10°, respectively.

Fig. 8. T_c and ρ_0 (20 K) vs the film thickness of NbN.

$$\lambda_{GL}^d(T) = 64.2[\rho_0(\mu\Omega \cdot cm)/T_c(K)]^{1/2}(1-T/T_c)^{-1/2} \quad (nm) \tag{2}$$

For strong coupling, the theoretical $\lambda(T)$ is expressed by[19]

$$\lambda(T) = 1.63\eta(T)\lambda_{GL}^d(T). \tag{3}$$

Using these equations and the measured average value of T_c and ρ_0, we calculated the theoretical values of $\lambda_{GL}^d(0)$ and $\lambda(0)$. We assumed that the factor $\eta(4.2$ K) is 0.91 for NbN,[18] and $\lambda(0) = \lambda(T)[1-(T/T_c)^4]^{-1/2}$. Our films have a theoretical penetration depth of approximately $\lambda(0) \sim 300$ nm for NbN($\rho_0 = 140$ $\mu\Omega \cdot cm$, $T_c = 14$ K) of 10 nm thickness, and 228 nm for NbN($\rho_0 = 80$ $\mu\Omega \cdot cm$, $T_c = 14$ K) of 10 nm thickness. The $\lambda(0)$'s for epitaxial NbN of thickness less than 20 nm (ultrathin films) are relatively short in comparison with those reported by Igarashi *et al.*[18]

The experimental penetration depth, $\langle\lambda(4.2$ K)$\rangle_{av}$, was obtained by analyzing the flux modulation of the critical current in dc-SQUID with a NbN ground plane.[19] Using NbN/MgO/NbN junction technology described elsewhere,[21] dc-SQUIDs were fabricated. Figure 9 shows the schematic configuration with a NbN ground plane (a) and equivalent circuit of the dc-SQUID (b). Typical flux modulation of the interferometer is shown in Fig. 9(c) as a function of applied magnetic flux which is produced by control current I_c as shown in Fig. 9(a). The strip line inductance L may be calculated from the measured control
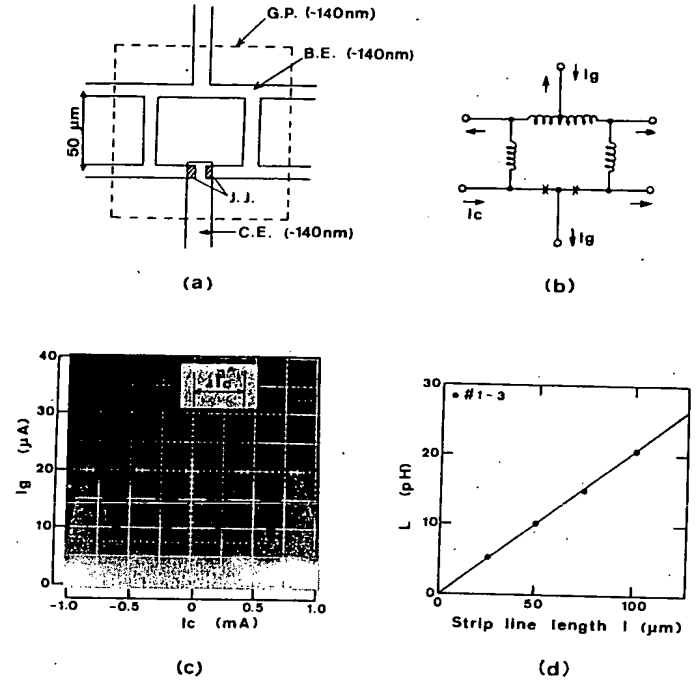

Fig. 9. (a) Schematic configuration of a direct coupled dc-SQUID with a NbN ground plane. (b) Equivalent circuit. (c) Typical flux modulation of a two junction interferometer. (d) Strip inductance vs the strip line length.

current shift ΔI_c between the quantum states as $L = \Phi_0/\Delta I_c$,[22] where $\Phi_0(hc/2e=2.07 \times 10^{-7}$ G $\cdot$ cm$^2)$ is the flux quantum. Figure 9(d) shows the inductance L as a function of the line length l. In the calculation of $\lambda_{th}(4.2$ K), we assumed $\eta(4.2$ K) ~ 0.91.

As seen in Table I, the penetration depth in NbN films varies widely, obscuring interpretation of the data. The average value $\langle\lambda_{ex}(4.2$ K)$\rangle_{av}$ is, however, in close agreement with the calculated value $\langle\lambda_{th}(4.2$ K)$\rangle_{av}$. The short penetration depth of epitaxial NbN films may decrease the kinetic inductance of NbN electrodes, resulting in an increase in the magnetic sensitivity of SQUID

*The strip inductance L in dc-SQUID with a ground plane is given by $L = \mu_0(ld_0/W)[1+(\lambda_g/d_0)\coth(d_g/\lambda_g)+(\lambda_b/d_0)\coth(d_b/\lambda_b)]$, where W is the width of the line and l is the line length, and λ_g and λ_b are the superconducting penetration depth of the ground plane and strip line. The d_g and d_b are also the thicknesses of the ground plane and line, respectively, and μ_0 is the permeability of free space. In this study, $W \gg d_0 + \lambda_g + \lambda_b$ and $d_g \sim d_b$. So, the fringing field can be neglected. We assume $\lambda_g = \lambda_b (\equiv \langle\lambda\rangle_{av})$, and calculate $\langle\lambda(4.2$ K)$\rangle_{av}$ from the measured strip inductance.

Table I. Superconducting parameters of epitaxial NbN films.

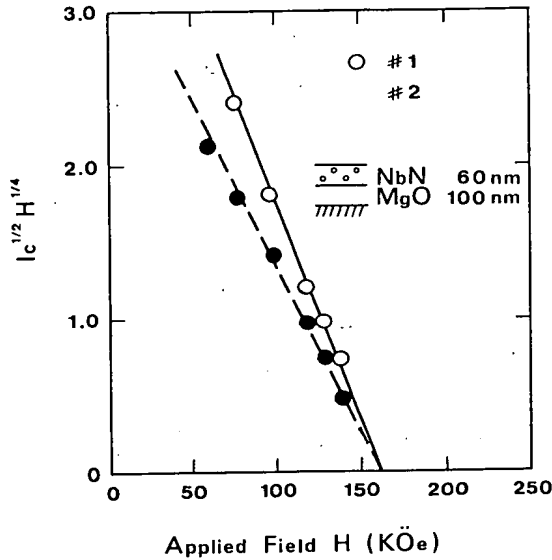| Sample No.	T_c (K)		ρ_0(20 K) ($\mu\Omega \cdot cm$)		$\lambda(4.2$ K) (nm)		L (pH/μm)	$\langle\lambda(4.2$ K)$\rangle_{av}$ (nm)
	G.P.[a]	B.[b]	G.P.[a]	B.[b]	G.P.[a]	B.[b]		
#1	15.5	15.3	188	209	388	413	0.21	401
#2	14.9	15.0	129	177	331	386	0.21	358
#3	15.3	15.9	117	187	309	380	0.21	343

a) Ground Plane
b) Base Electrode

Fig. 10. Parameter $I_c^{1/2}H^{1/4}$ vs external magnetic field H for NbN.

magnetometers[23] and decrease in the propagation delay of the microstrip transmission line.[20]

One method for estimating the GL coherence length, ξ, is to measure the upper critical field H_{c2}. In the GL theory of Type II superconductivity, ξ is expressed by the well-known formula[24]

$$\xi = (\Phi_0/2H_{c2})^{1/2}. \qquad (4)$$

To obtain the order of magnitude of ξ, we measured the critical current, I_c, as a function of applied field, H, at 4.2 K. The resistive measurement of I_c was carried out in a 16.5 T superconducting magnet in Tohoku University. I_c was defined by 2 μV/cm. According to Kramer's flux-pinning theory,[25] the $I_c^{1/2}H^{1/4}$ is expressed in the form given by

$$I_c^{1/2}H^{1/4} \propto 1 - H/H_{c2}. \qquad (5)$$

Therefore, the plot of this product on applied field should be a straight line intercepting the abscissa at $H=H_{c2}$.

Figure 10 shows the $I_c^{1/2}H^{1/4}$-vs-H plots for two NbN films of ~60 nm thickness. The field is parallel to the film surface. We found that the anisotropy of H_{c2} in our epitaxial NbN films is less than 10%. The $I_c^{1/2}H^{1/4}$-vs-H curves are approximately linear, and the obtained $H_{c2}(4.2 \text{ K})$ is 160 KOe. The GL coherence length estimated from eq. 4 ξ(4.2 K) is ~4.5 nm. This value is somewhat larger than the reported value for NbN on a single crystal sapphire substrate.[26]

§5. Conclusions

Using an rf magnetron sputtering system with a diffusion-pump or cryo-pump, high-T_c NbN thin films were successfully prepared on MgO underlayers. The microstructure was analyzed by XTEM, HEED and XRD, and heteroepitaxial growth (NbN(100)//MgO (100)) was confirmed in NbN films and NbN/MgO/NbN trilayers deposited on the (200) oriented MgO underlayer. Using the GL theory and the measured

values of T_c and ρ_0, we calculated the GL parameters of $\lambda(0)$ and ξ for epitaxial NbN films. The epitaxial NbN thin films had high T_c's, relatively low residual resistivities, considerably short GL penetration depth and long coherence length. The epitaxial growth technique presented in this study will be useful for the preparation of Josephson devices, such as tunnel junctions or nanobridges.

References

1) A. I. Braginski, J. R. Gavaler, M. A. Janocko and J. Talvacchio: SQUID 85, eds., H. D. Hahlbohm and H. Lubbig, (Walter de Gruyter, Berlin 1985) p. 591.
2) G. Oya and Y. Onodera: Jpn. J. Appl. Phys. 10 (1971) 1485.
3) G. Oya and Y. Onodera: J. Appl. Phys. 45 (1974) 1389.
4) Y. M. Shy, L. E. Toth and R. Somasundaram: J. Appl. Phys. 44 (1973) 5539.
5) S. Kosaka and Y. Onodera: Proc. 6th Int. Vaccum Congress, Kyoto, 1974, Jpn. J. Appl. Phys. 13 (1974) Suppl. 2, Pt 1, p. 613.
6) J. R. Gavaler, A. I. Braginski, M. A. Janocko and J. Talvacchio: Physica 135B (1985) 148.
7) K. Ueda, K. Hamasaki, I. Yamada, T. Yamashita, T. Komata and Y. Hirukawa: Shinku 28 (1985) 796 (in Japanese).
8) T. Yamashita, K. Hamasaki and T. Komata: Adv. Cryog. Eng. 32 (1986) 617.
9) J. Talvacchio, J. R. Gavaler and A. I. Braginski: to be published in Proc. TMS-AIME: Metallic Multilayers and Epitaxy, eds. H. Hong and S. A. Wolf (1987).
10) J. Talvacchio and A. I. Braginski: Extended Abstracts of the 1987 Int. Superconductivity Electronics Conference (ISEC), (1987) p. 66.
11) W. R. Sinclair and C. J. Calbick: Appl. Phys. Lett. 10 (1967) 214.
12) S. Nagaoka, K. Hamasaki, T. Yamashita and T. Komata: IEICE Tech. Rep. SCE86-12 (1986) 1 (in Japanese).
13) K. Sugiyama, K. Akazawa, M. Oshima, H. Miura, T. Matsuda and O. Nomura: Plasma Chem. & Plasma Processing 6 (1986) 179.
14) L. Hochard, A. Plain and A. Ricard: Proc. 4th Int. Symp. Plasma Chem., ed. by S. Veprek (University Zurich) (1979) p. 545.
15) K. Hamasaki, S. Nagaoka, T. Komata and T. Yamashita: Superconducting Materials, Extended Abstracts, eds. J. Beuk and A. I. Braginski (Materials Res. Soc., Pittsburg, 1986) p. 10.
16) K. Yachi, K. Hamasaki, T. Yamashita and S. Nagaoka: IEICE Tech. Rep. SCE86-39 (1986) 41 (in Japanese)
17) J. R. Gavaler, J. Talvacchio and A. I. Braginski: Adv. Cryog. Eng. 30 (1984) 535.
18) M. Igarashi, M. Hikita and K. Takei: Adv. Cryog. Eng. 30 (1984) 627.
19) T. P. Orlando, E. J. McNiff, S. Foner and M. R. Beasley: Phys. Rev. B19 (1979) 4545.
20) T. R. Gheewala: IBM J. Res. & Develop. 24 (1980) 130.
21) K. Ueda, I. Yamada, K. Hamasaki, T. Komata and T. Yamashita: IEICE Tech. Rep. SCE85-2 (1985) 7 (in Japanese).
22) H. H. Zappe and B. S. Landman: J. Appl. Phys. 49 (1978) 344.
23) J. Clarke: IEEE Trans. Electron Devices ED-27 (1980) 1896.
24) F. E. Harper and M. Tinkham: Phys. Rev. 172 (1968) 441.
25) E. J. Kramer: J. Appl. Phys. 44 (1973) 1360.
26) J. Y. Juang, D. A. Rudman, R. B. van Dover, W. R. Sinclair and D. D. Bacon: Adv. Cryog. Eng. 32 (1986) 651.